Energy transfer dynamics in strongly inhomogeneous hot-dense-matter systems

C. R. Stillman, P. M. Nilson, A. B. Sefkow, S. T. Ivancic, C. Mileham, I. A. Begishev, and D. H. Froula

Phys. Rev. E **97**, 063208 — Published 25 June 2018

DOI: 10.1103/PhysRevE.97.063208

Energy Transfer Dynamics in Strongly Inhomogeneous Hot-Dense-Matter Systems

C. R. Stillman[1, 2], P. M. Nilson[1], A. B. Sefkow[1,2,3], S. T. Ivancic[1], C. Mileham[1], I. A. Begishev[1], and D. H. Froula[1, 2]

[1]Laboratory for Laser Energetics, University of Rochester, 250 East River Road, Rochester NY 14623, USA

[2]Department of Physics and Astronomy, University of Rochester, Rochester NY 14627, USA

[3]Department of Mechanical Engineering, University of Rochester, Rochester NY 14623, USA

Direct measurements of energy transfer across steep density and temperature gradients in a hot-dense-matter system are presented. Hot dense plasma conditions were generated by high-intensity laser irradiation of a thin-foil target containing a buried metal layer. Energy transfer to the layer was measured using picosecond time-resolved x-ray emission spectroscopy. The data show two x-ray flashes in time. Fully explicit, coupled particle-in-cell and collisional-radiative atomic kinetics model predictions reproduce these observations, connecting the two x-ray flashes with staged radial energy transfer within the target.

[1]Email: csti@lle.rochester.edu

I. INTRODUCTION

Hot dense plasma states are generated and controlled by intense energy flows in conditions far from thermal equilibrium. These states are prevalent in controlled thermonuclear fusion research [1], high-energy-density science [2], and astrophysical plasma studies [3]. Energy transfer dynamics relevant to these systems are challenging to recreate and measure in the laboratory and require the confinement of powerful energy fluxes [4]. In such extreme conditions, prompt energy deposition can be mediated by intense radiation flows [5], strong electromagnetic currents [6], and energetic particle beams [7]. The complex interplay between these processes and a material as it responds to intense heating is the subject of extensive study [8–12].

Experimental techniques using optimized drive conditions [13] and embedded thin sample layers [14] have been widely developed to control the formation of simultaneously hot, uniform, and dense plasmas. While such homogeneous conditions are typically sought for broad applications, such as opacity and equation-of-state studies of stellar-interior matter [15,16], purposefully driving energy density inhomogeneities is fundamental to understanding the behavior of high-temperature and far-from-equilibrium systems. Predicting how material properties change under intense heating accompanied by thermal decompression is a crucial part of this work [17]. In the strongly inhomogeneous regime, data are sparse and theoretical modeling is difficult [18], requiring spatially, spectrally, and temporally resolved measurements to test detailed energy transport and radiation–hydrodynamic model predictions [19–22].

This paper reports picosecond time-resolved measurements of energy transfer across steep density and temperature gradients in hot dense matter. These experiments show, for the first time, two time-resolved x-ray flashes from a heated buried sample. Hot electrons generated by a tightly focused high-intensity laser pulse heated the center of a plastic foil containing a thin

Al or Al/Fe-admixture metal layer. Energy-transfer dynamics were inferred from picosecond time-resolved measurements of the Al He_α thermal line and broadband x-ray emission using a two-dimensional (2-D), fully explicit particle-in-cell (PIC) [23] and collisional-radiative atomic kinetics model [24]. The two flashes were caused by hot-electron–driven heating of the central volume followed by radial nonequilibrium energy transfer to a surrounding dense annulus. The Fe admixture slows the radial energy transfer, allowing one to measure a second time-resolved x-ray flash from the heated annulus. This staged energy coupling within the target is governed spatially and temporally by the hydrodynamic disassembly of the center of the target. The observations impose new stringent constraints for testing heating model predictions in warm and hot dense matter. This work contributes novel data toward the fundamental science needed to understand the time-dependent response of materials to intense energy flows in order to predict the behavior of extreme high-energy-density systems.

II. EXPERIMENT DETAILS

The experiments were carried out at the Multi-Terawatt (MTW) Laser Facility [25] at the University of Rochester's Laboratory for Laser Energetics. The laser directly irradiated thin-foil targets with 10- or 15-J, 0.7-ps pulses at the laser's fundamental wavelength (λ = 1054 nm). The laser was focused to an ~5-μm full-width-at-half-maximum (FWHM) focal spot by an *f*/3.3 off-axis parabolic mirror at normal incidence to the target at intensities greater than 10^{18} W/cm^2. The measured temporal contrast of the laser is 10^8 up to 100 ps prior to the main pulse [26].

The targets were 200-μm-diam plastic foils with a concentric buried Al or Al/Fe microdot that was 100 μm in diameter [14]. The large microdot radius relative to the laser focal spot accentuates the energy transfer dynamics across sharp temperature and density gradients. The

microdot was vacuum deposited as a 0.2-μm thin layer on a 1-μm parylene-N support. The Al/Fe admixture was deposited from a uniformly co-mixed alloy consisting of 50 at. % Al and 50 at. % Fe. A 2-μm parylene overcoat was applied to the front of each target to constrain hydrodynamic expansion of the buried layer. The microdot is purposefully thin in order to limit spatial gradients and optical depth effects in the longitudinal direction [27].

An ultrafast streaked x-ray spectrometer measured the Al He_α thermal line emission and the emergent broadband radiation between 1590 and 1660 eV. The spectrometer uses a high-throughput conically curved potassium acid phthalate (KAP) crystal to focus x rays to the input slit of a picosecond x-ray streak camera. The measured streak camera impulse response was 2 ps and the temporal axis was calibrated in separate tests [8]. The spectral resolving power of the instrument is $E/\Delta E \approx 1000$.

III. RESULTS

Figures 1(a) and 1(b) show time-resolved Al He_α thermal line and broadband emission from buried Al or Al/Fe microdots that were irradiated by 15-J, 0.7-ps pulses at focused intensities near 1×10^{19} W/cm^2. Relatively low signal levels observed from the Al/Fe experiment result from the decreased concentration of Al ions and, importantly, suggest that the Fe admixture reduces the plasma temperature of the sample layer. Radiation transfer calculations using an escape probability approach [24] show that the admixture Fe ions are optically thin to the Al He_α. The images reveal strong initial broadband emission relative to the Al He_α when Fe is present in the layer because of strong bremsstrahlung emission during the hot-electron pulse and enhanced blackbody radiation at late times.

Spectrally integrated data in the He_α and broadband spectral bands are displayed below the streak images to show the time-dependent x-ray emission from both targets. The pure-Al data [Fig. 1(c)] is characterized by a single x-ray flash in the He_α and broadband spectral ranges. The broadband emission and He_α intensify simultaneously—implying hot-electron heating—and exhibit similar temporal profiles.

In contrast, two distinct He_α flashes are observed when Fe is added to the layer [Fig. 1(d)]. As with the pure-Al target, the first He_α flash rises promptly with the broadband emission, indicating that it is coincident with the hot-electron pulse. X-ray emission in both bands re-emerges at roughly t_0 + 20 ps, where t_0 is the arrival time of the high-intensity laser pulse. This is particularly prominent in the Al He_α band, but enhancement of the falling edge in the broadband emission is evident. The prolonged duration of the second flash relative to the first suggests that significant energy transfer occurs after the initial hot-electron energy deposition.

Figure 2 shows additional data that confirm the observations at lower laser intensity. Dashed lines represent He_α emission from pure-Al buried layers. Single x-ray flashes consistent with previous studies [4,20–22] were measured in each Al-only experiment. The temporal profiles were generally symmetric with a slight softening of the falling edge. The data have been scaled by the indicated factor for comparison to the Al/Fe-admixture data (black and blue points).

Raw lineouts measured from the Al/Fe-admixture data are fit by a pair of exponentially modified Gaussian functions to characterize the temporal dynamics. Shaded regions display the 95% confidence interval for the best fit including simultaneous uncertainty in the fit parameters and statistical uncertainty in the measured signal. Two separate x-ray flashes are evident in the He_α and broadband data and are nearly coincident across spectral bands. The fast rise time of the

first flash broadly tracks the early x-ray emission measured from pure-Al targets. In each case, x-ray emission measured from Al/Fe-admixture samples continues for ≳25 ps after emission from the corresponding pure-Al experiment. Importantly, the temporal separation between the two flashes increases for lower laser intensities.

IV. MODELING AND INTERPRETATION

Fully explicit, kinetic, electromagnetic, and relativistic particle-in-cell (PIC) calculations using the *LSP* code [23,28] were carried out for the targets irradiated by 10-J, 0.7-ps laser pulses. The 2-D PIC simulations were initialized with a realistic preplasma profile based on radiation–hydrodynamic modeling of the measured MTW prepulse up to an intensity of 10^{17} W/cm^2 [29]. The laser-irradiation geometry, including f number and focal spot size, was reproduced in the PIC model. The code launched electromagnetic waves from the simulation boundary and therefore modeled the laser–plasma interaction self-consistently without prescribing an *ad hoc* electron energy distribution. This fully explicit scheme does not admit physical approximations, in contrast to implicit, hybrid fluid-kinetic, or electron-injection PIC methods. The plasma density and mean ionization state were evolved in conjunction with an inline particle-based radiation package for accurate hot-electron energy coupling and transport. The model includes proton acceleration by quasi-static external sheath fields [target normal sheath acceleration (TNSA)] [29] and was extended up to 100 ps after the high-intensity interaction.

The simulation results for Al/Fe and pure-Al tracer layers with 2-μm plastic overcoats are presented in Fig. 3. Figure 3(a) shows the spatially resolved electron density 20 ps after the high-intensity laser interaction. The original position of the tracer layer is indicated by the shaded rectangle. The center of the target has disassembled, leaving intact a colder outer annulus. Detail views of the tracer ion density and bulk electron temperature are presented in 10-ps intervals for

Al/Fe and pure-Al tracers in Figures 3(b)–3(e) and figs. 3(f)–3(i), respectively, between 10 and 40 ps after the laser pulse. The images show rapid decompression at the center of the buried layer and highlight the extended period of time that the Al/Fe layer remains intact relative to the pure-Al case. A well-defined annulus is clearly present in the Al/Fe sample while the pure-Al layer has largely disassembled by 40 ps. The spatially resolved electron temperatures show sharp variation along the radial direction and strongly inhomogeneous energy density conditions.

The steep radial temperature gradient between the on-axis material and the outer annulus is formed by localized hot-electron–driven heating on the laser axis. This temperature gradient drives strong transverse energy transfer to the colder, dense annulus. The present experiment accentuates this secondary heating stage by minimizing the size of the laser focal spot relative to the buried-layer radius and by including Fe ions in the tracer material.

Admixture Fe ions reduce the peak temperatures achieved in the experiment and dramatically slow the hydrodynamic decompression of the buried layer, allowing the on- and off-axis heating stages to be temporally resolved. Compared to the pure-Al layers, the Al/Fe admixtures heat gradually and exhibit relaxed temperature gradients. The reduced temperature gradient slows the radial energy transfer, giving the on-axis material time to heat and decompress—forming the first x-ray flash—before the outer annulus heats and emits the second x-ray flash. The first x-ray flash is truncated by rapid high-pressure release of the on-axis material prior to significant energy transfer to the remaining warm dense annulus. Temporal separation between the two flashes is sensitive to the release properties of the on-axis material relative to the energy transfer rate to the outer annulus. The lower temperature and increased inertia of the relatively massive Fe ions keep the annulus intact long enough to observe the energy transfer dynamics and the second x-ray flash.

Calculated time-resolved temperatures and densities spatially averaged over each region of the target were provided to a fully time-dependent collisional-radiative atomic kinetics model to estimate the time-resolved He_α emission [24]. Separate atomic kinetics calculations for the on- and off-axis material were combined to account for spatial integration in the streaked measurement. The calculated Al He_α signal (blue) is compared to the measured data (black) in Figs. 4(a) and 4(b) for the Al/Fe and pure-Al tracers respectively. In general, the calculated He_α signal agrees with the data from both Al/Fe and pure-Al tracers within the 95% confidence interval (shaded bands). Simulations of the Al/Fe admixture reproduce the sharp rising edge of the initial flash and capture the slower rise time of the second flash from the off-axis material. The temporal delay and decay time of the two x-ray flashes is similarly well matched, indicating that the material release and evolution are being modeled sufficiently to permit straightforward identification of the energy transfer dynamics.

Simulations for pure-Al layers broadly reproduce the single flashes observed in the experiments [Fig. 4(b)]. The single flash is composed of coincident emission from the inner and outer regions of the target; rapid energy transfer to the outer annulus prevents two distinct flashes in time. The falling edge of the first flash and the rising edge of the second flash add in such a way to reproduce the measured rising edge. The energy radiated from the Al targets emanates predominantly from the second flash and is ultimately truncated by hydrodynamic release. The peak calculated He_α intensity from the pure-Al targets is ~12× greater than that from the Al/Fe admixture, reasonably close to the ~14× factor observed in the experiment [Fig. 2(a)].

V. SUMMARY

In summary, energy transfer properties of hot, dense, and inhomogeneous plasmas have been observed with picosecond time-resolved x-ray spectroscopy. Energy transport was studied by purposefully accentuating spatial gradients inside the plasma and time-resolving the plasma emission, providing new experimental insight into the behavior of hot dense matter and the intense energy flows that are required to create it. The observed energy transfer dynamics are widely applicable to hot dense matter studies with all high-energy-density drivers, including x-ray free-electron lasers [30], high-current *Z*-pinches [31], and direct and indirect lasers [32]. The data show two reproducible, distinct x-ray flashes in time, signaling sequential phases in the energy transfer dynamics and material response to intense heating. The experimental observations are consistent with fully explicit, parameter-free particle-in-cell and collisional-radiative atomic model predictions that connect the two x-ray flashes with hot-electron and return-current heating of on-axis material, followed by radial energy transfer to the surrounding dense matter. The results strongly motivate future studies of the energy transport properties of complex mixtures or high-*Z* atomic systems subject to intense heating. An improved understanding of how energy density inhomogeneities form and evolve in such hot-dense-matter systems will help improve the design and interpretation of all high-temperature plasma opacity and equation-of-state studies.

Acknowledgement

This material is based upon work supported by the Department of Energy National Nuclear Security Administration under Award No. DE-NA0001944 and the office of Fusion Energy Sciences under Award No. DE-SC0012317.

This report was prepared as an account of work sponsored by an agency of the U.S. Government. Neither the U.S. Government nor any agency thereof, nor any of their employees,

makes any warranty, express or implied, or assumes any legal liability or responsibility for the accuracy, completeness, or usefulness of any information, apparatus, product, or process disclosed, or represents that its use would not infringe privately owned rights. Reference herein to any specific commercial product, process, or service by trade name, trademark, manufacturer, or otherwise does not necessarily constitute or imply its endorsement, recommendation, or favoring by the U.S. Government or any agency thereof. The views and opinions of authors expressed herein do not necessarily state or reflect those of the U.S. Government or any agency thereof.

References

[1] R. Betti and O. A. Hurricane, Nat. Phys. **12**, 435 (2016); M. R. Gomez, S. A. Slutz, A. B. Sefkow, D. B. Sinars, K. D. Hahn, S. B. Hansen, E. C. Harding, P. F. Knapp, P. F. Schmit, C. A. Jennings *et al.*, Phys. Rev. Lett. **113**, 155003 (2014); R. Kodama, P. A. Norreys, K. Mima, A. E. Dangor, R. G. Evans, H. Fujita, Y. Kitagawa, K. Krushelnick, T. Miyakoshi, N. Miyanaga *et al.*, Nature **412**, 798 (2001).

[2] M. K. Matzen, M. A. Sweeney, R. G. Adams, J. R. Asay, J. E. Bailey, G. R. Bennett, D. E. Bliss, D. D. Bloomquist, T. A. Brunner, R. B. Campbell *et al.*, Phys. Plasmas **12**, 055503 (2005); E. I. Moses, R. N. Boyd, B. A. Remington, C. J. Keane, and R. Al-Ayat, Phys. Plasmas **16**, 041006 (2009).

[3] B. A. Remington, D. Arnett, R. P. Drake, and H. Takabe, Science **284**, 1488 (1999); D. A. Uzdensky and S. Rightley, Rep. Prog. Phys. **77**, 036902 (2014).

[4] C. R. D. Brown, D. J. Hoarty, S. F. James, D. Swatton, S. J. Hughes, J. W. Morton, T. M. Guymer, M. P. Hill, D. A. Chapman, J. E. Andrew *et al.*, Phys. Rev. Lett. **106**, 185003 (2011); A. Saemann, K. Eidmann, I. E. Golovkin, R. C. Mancini, E. Andersson, E. Förster, and K. Witte, Phys. Rev. Lett. **82**, 4843 (1999).

[5] R. Cauble, L. B. Da Silva, Jr T. W. Barbee, P. Celliers, J. C. Moreno, and A. S. Wan, Phys. Rev. Lett. **74**, 3816 (1995); A. Lévy, P. Audebert, R. Shepherd, J. Dunn, M. Cammarata, O. Ciricosta, F. Deneuville, F. Dorchies, M. Fajardo, C. Fourment *et al.*, Phys. Plasmas **22**, 030703 (2015).

[6] X. Ribeyre, S. Gus'kov, J.-L. Feugeas, Ph. Nicolaï, and V. T. Tikhonchuk, Phys. Plasmas **20**, 062705 (2013).

[7] P. K. Patel, A. J. Mackinnon, M. H. Key, T. E. Cowan, M. E. Foord, M. Allen, D. F. Price, H. Ruhl, P. T. Springer, and R. Stephens, Phys. Rev. Lett. **91**, 125004 (2003); P. M. Nilson, A. A. Solodov, J. F. Myatt, W. Theobald, P. A. Jaanimagi, L. Gao, C. Stoeckl, R. S. Craxton, J. A. Delettrez, B. Yaakobi *et al.*, Phys. Rev. Lett. **105**, 235001 (2010).

[8] P. M. Nilson, J. R. Davies, W. Theobald, P. A. Jaanimagi, C. Mileham, R. K. Jungquist, C. Stoeckl, I. A. Begishev, A. A. Solodov, J. F. Myatt *et al.*, Phys. Rev. Lett. **108**, 085002 (2012).

[9] A. Frank, A. Blažević, V. Bagnoud, M. M. Basko, M. Börner, W. Cayzac, D. Kraus, T. Heßling, D. H. H. Hoffmann, A. Ortner *et al.*, Phys. Rev. Lett. **110**, 115001 (2013).

[10] Y. Ping, A. Fernandez-Panella, H. Sio, A. Correa, R. Shepherd, O. Landen, R. A. London, P. A. Sterne, H. D. Whitley, D. Fratanduono *et al.*, Phys. Plasmas **22**, 092701 (2015).

[11] K. U. Akli, S. B. Hansen, A. J. Kemp, R. R. Freeman, F. N. Beg, D. C. Clark, S. D. Chen, D. Hey, S. P. Hatchett, K. Highbarger *et al.*, Phys. Rev. Lett. **100**, 165002 (2008).

[12] S. Gus'kov, X. Ribeyre, M. Touati, J. L. Feugeas, Ph. Nicolaï, and V. Tikhonchuk, Phys. Rev. Lett. **109**, 255004 (2012).

[13] S. M. Vinko, O. Ciricosta, B. I. Cho, K. Engelhorn, H. K. Chung, C. R. D. Brown, T. Burian, J. Chalupsky, R. W. Falcone, C. Graves *et al.*, Nature **482**, 59 (2012).

[14] G. J. Tallents, M. H. Key, P. Norreys, D. Brown, J. Dunn, and H. Baldis, Phys. Rev. A **40**, R2857 (1989).

[15] J. E. Bailey, T. Nagayama, G. P. Loisel, G. A. Rochau, C. Blancard, J. Colgan, Ph. Cosse, G. Faussurier, C. J. Fontes, F. Gilleron *et al.*, Nature **517**, 56 (2015); T. S. Perry, S. J. Davidson, F. J. D. Serduke, D. R. Bach, C. C. Smith, J. M. Foster, R. J. Doyas, R. A. Ward, C. A. Iglesias, F. J. Rogers *et al.*, Phys. Rev. Lett. **67**, 3784 (1991).

[16] J. Christensen-Dalsgaard, W. Däppen, S. V. Ajukov, E. R. Anderson, H. M. Antia, S. Basu, V. A. Baturin, G. Berthomieu, B. Chaboyer, S. M. Chitre *et al.*, Science **272**, 1286 (1996); W. Däppen and J. A. Guzik, in *Variable Stars as Essential Astrophysical Tools*, NATO Science Series (Series C: Mathematical and Physical Sciences), edited by İ. C. (Springer, Dordrecht, 2000), Vol. 544, p. 177.

[17] E. Brambrink, T. Schlegel, G. Malka, K. U. Amthor, M. M. Aléonard, G. Claverie, M. Gerbaux, F. Gobet, F. Hannachi, V. Méot *et al.*, Phys. Rev. E **75**, 065401 (2007); K. L. Lancaster, A. P. L. Robinson, J. Pasley, P. Hakel, T. Ma, K. Highbarger, F. N. Beg, S. N. Chen, R. L. Daskalova, R. R. Freeman *et al.*, Phys. Plasmas **24**, 083115 (2017).

[18] Z. Chen, V. Sametoglu, Y. Y. Tsui, T. Ao, and A. Ng, Phys. Rev. Lett. **108**, 165001 (2012).

[19] P. Audebert, P. Renaudin, S. Bastiani-Ceccotti, J.-P. Geindre, C. Cheanis-Popovics, S. Tzortzakis, V. Nagels-Silvert, R. Shepherd, I. Matsushima, S. Gary *et al.*, Phys. Rev. Lett. **94**, 025004 (2005).

[20] J. A. Koch, M. H. Key, R. R. Freeman, S. P. Hatchett, R. W. Lee, D. Pennington, R. B. Stephens, and M. Tabak, Phys. Rev. E **65**, 016410 (2001).

[21] R. G. Evans, E. L. Clark, R. T. Eagleton, A. M. Dunne, R. D. Edwards, W. J. Garbett, T. J. Goldsack, S. James, C. C. Smith, B. R. Thomas *et al.*, Appl. Phys. Lett. **86**, 191505 (2005).

[22] D. J. Hoarty, N. Sircombe, P. Beiersdorfer, C. R. D. Brown, M. P. Hill, L. M. R. Hobbs, S. F. James, J. Morton, E. Hill, M. Jeffery *et al.*, High Energy Density Phys. **23**, 178 (2017).

[23] A. B. Sefkow, G. R. Bennett, M. Geissel, M. Schollmeier, B. C. Franke, and B. W. Atherton, Phys. Rev. Lett. **106**, 235002 (2011).

[24] J. J. MacFarlane, I. E. Golovkin, P. Wang, P. R. Woodruff, and N. A. Pereyra, High Energy Density Phys. **3**, 181 (2007).

[25] V. Bagnoud, I. A. Begishev, M. J. Guardalben, J. Puth, and J. D. Zuegel, Opt. Lett. **30**, 1843 (2005).

[26] C. Dorrer, A. Consentino, D. Irwin, J. Qiao, and J. D. Zuegel, J. Opt. **17**, 094007 (2015).

[27] T. S. Perry, P. T. Springer, D. F. Fields, D. R. Bach, F. J. D. Serduke, C. A. Iglesias, F. J. Rogers, J. K. Nash, M. H. Chen, B. G. Wilson *et al.*, Phys. Rev. E **54**, 5617 (1996).

[28] T. P. Hughes, R. E. Clark, and S. S. Yu, Phys. Rev. ST Accel. Beams **2**, 11040 (1999).

[29] M. Schollmeier, A. B. Sefkow, M. Geissel, A. V. Arefiev, K. A. Flippo, S. A. Gaillard, R. P. Johnson, M. W. Kimmel, D. T. Offermann, P. K. Rambo *et al.*, Phys. Plasma **22**, 043116 (2015).

[30] T. R. Preston, S. M. Vinko, O. Ciricosta, P. Hollebon, H. K. Chung, G. L. Dakovski, J. Krzywinski, M. Minitti, T. Burian, J. Chalupský *et al.*, Phys. Rev. Lett. **119**, 085001 (2017).

[31] M. K. Matzen, Phys. Plasmas **4**, 1519 (1997); A. B. Sefkow, S. A. Slutz, J. M. Koning, M. M. Marinak, K. J. Peterson, D. B. Sinars, and R. A. Vesey, Phys. Plasmas **21**, 072711 (2014); S. B. Hansen, M. R. Gomez, A. B. Sefkow, S. A. Slutz, D. B. Sinars, K. D. Hahn, E. C. Harding, P. F. Knapp, P. F. Schmit, T. J. Awe *et al.*, Phys. Plasmas **22**, 056313 (2015).

[32] J. Nuckolls, L. Wood, A. Thiessen, and G. Zimmerman, Nature **239**, 139 (1972).

Figures

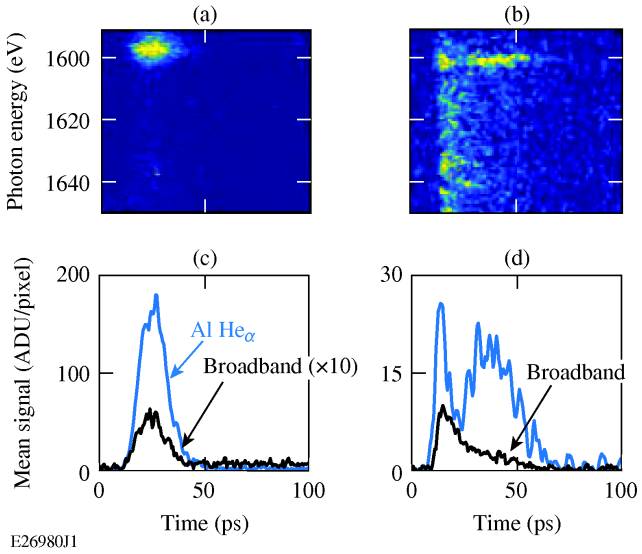

FIG. 1. Time-resolved data from (a) pure-Al and (b) Al/Fe-admixture targets. The spectrally integrated temporal evolution of the Al He$_\alpha$ (blue) and broadband emission (black) is shown for the (c) pure-Al and (d) Al/Fe cases. The broadband emission in (c) has been scaled by a factor of 10 for presentation clarity.

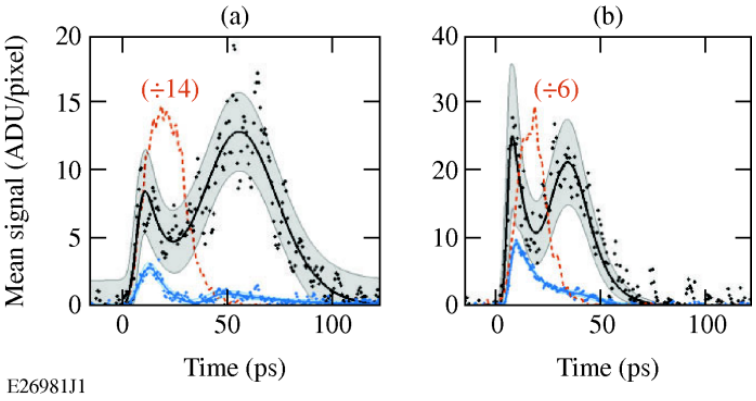

FIG. 2. Simultaneous He$_\alpha$ (black) and broadband (blue) emission from Al/Fe admixtures. Scaled pure-Al data (orange) are overlaid for comparison. The irradiation conditions were (a) 10 J, 0.7 ps; (b) 15 J, 0.7 ps.

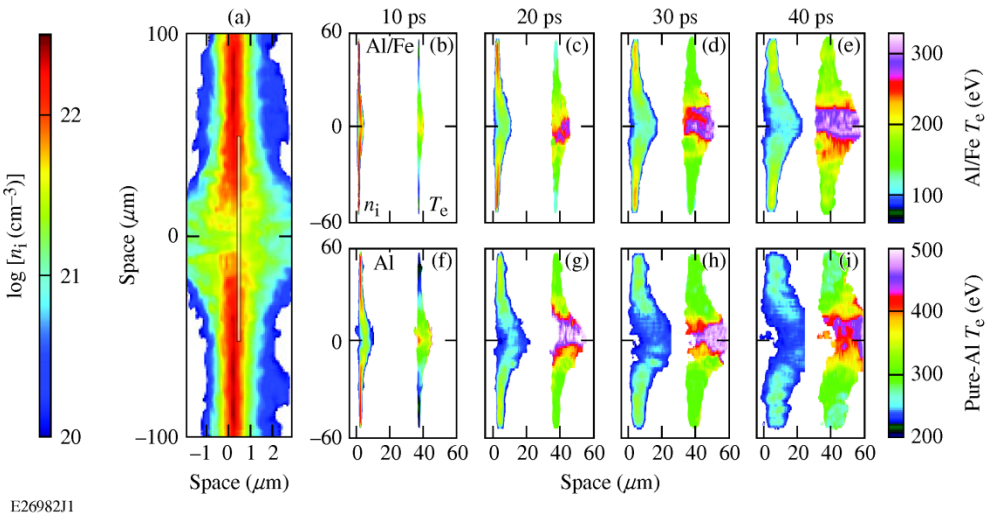

FIG. 3. (a) The spatially resolved electron density is shown for the entire target at t_0 + 20 ps for the pure-Al case. The shaded region is the initial location of the buried tracer. Detail views of the spatially resolved ion density and electron temperature in the Al/Fe tracer [(b)–(e)] and Al tracer [(f)–(i)] are shown at 10-ps intervals. The laser pulse delivered 10 J in 0.7 ps to an ~5 μm (FWHM) focal spot. The temperature scales are shown separately at right for the Al/Fe-admixture and pure-Al cases.

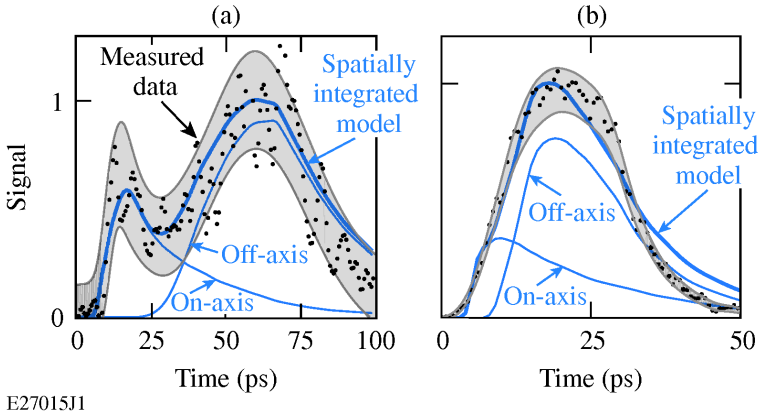

FIG 4. Time-dependent Al He$_\alpha$ radiation (blue) estimated from the PIC model is compared to the data (black) for the Al/Fe-admixture (a) and pure-Al (b) cases. Thin blue traces show the individual contributions from on- and off-axis material in the model.